

A jet model for Galactic black-hole X-ray sources: the cutoff energy–phase-lag correlation

P. Reig^{1,2}, and N. D. Kylafis^{2,1}

¹ IESL, Foundation for Research and Technology-Hellas, 711 10, Heraklion, Crete, Greece

² University of Crete, Physics Department & Institute of Theoretical & Computational Physics, 70013 Heraklion, Crete, Greece

Received:

Accepted:

ABSTRACT

Context. Galactic black-hole X-ray binaries emit a compact, optically thick, mildly relativistic radio jet when they are in the hard and hard-intermediate states, i.e., typically at the beginning and the end of an X-ray outburst. In a series of papers, we have developed a jet model and have shown, through Monte Carlo simulations, that our model can explain many observational results.

Aims. In this work, we investigate one more constraining relationship between the cutoff energy and the phase lag during the early stages of an X-ray outburst of the black-hole X-ray binary GX 339–4: the cutoff energy decreases while the phase lag increases during the brightening of the hard state.

Methods. We have performed Monte Carlo simulations of Compton upscattering of soft, accretion-disk photons in the jet and computed the phase lag between soft and hard photons and the cutoff energy of the resulting high-energy power law.

Results. We demonstrate that our jet model naturally explains the above correlation, with a minor modification consisting of introducing an acceleration zone at the base of the jet.

Conclusions. The observed correlation between the cutoff energy and the phase lag in the black-hole binary GX 339–4 suggests that the lags are produced by the hard component. Here we show that this correlation arises naturally if Comptonization in the jet produces these two quantities.

Key words. accretion, accretion disks – black hole physics – radiation mechanisms: non-thermal – methods: statistical – X-rays: stars

1. Introduction

The continuum X-ray spectra of black-hole binaries (BHB) are well described by just two components: i) a soft component, normally modeled as a multi-color black-body component dominating the spectrum below ~ 10 keV (Mitsuda et al. 1984; Merloni et al. 2000) and whose origin is attributed to a geometrically thin, optically thick disk (Shakura & Sunyaev 1973) and ii) a power-law hard tail with an exponential cutoff, which is believed to be the result of Comptonization of low-energy photons from the disk by energetic electrons in a configuration that is still under debate. The Comptonizing medium could be an optically thin, very hot “corona” in the vicinity of the compact object (Sunyaev & Titarchuk 1980; Hua & Titarchuk 1995; Zdziarski 1998), an advection-dominated accretion flow (Narayan & Yi 1994; Esin et al. 1997), a low angular momentum accretion flow (Ghosh et al. 2011; Garain et al. 2012), or the base of a radio jet (Band & Grindlay 1986; Georganopoulos et al. 2002). On top of these components, a discrete line at 6.4 keV is generally observed and attributed to reflection of the hard X-rays from the accretion disk (Fabian et al. 1989).

Based on the relative contribution of these two spectral components and the different shapes and characteristic frequencies of the noise components in the power spectra, including quasi-periodic oscillations (QPO), black-hole systems can be found in several states (McClintock & Remillard 2006; Belloni

2010), of which the two main ones are called soft and hard states (Done et al. 2007). In the soft state, the thermal black-body component dominates the energy spectrum with no or very weak power-law emission (Remillard & McClintock 2006; Dexter & Quataert 2012). Weak power-law noise (rms $< 5\%$) is detected in the power spectrum and sometimes a QPO at 10–20 Hz (van der Klis 2006). In the hard state, the soft component is weak or absent, whereas the hard tail extends to a few hundred keV in the form of a power law with photon-number index in the range 1.5 – 2. The power law falls exponentially at a few tens to about a hundred keV (McClintock & Remillard 2006; Castro et al. 2014). The power spectrum shows strong band-limited noise with a typical strength of 20% – 40% rms and a break frequency below 1 Hz (Homan & Belloni 2005; Belloni & Stella 2014). In addition, the existence of phase (time) lag between the light curves at two different energy bands obtained simultaneously is well established. The magnitude of this lag strongly depends on Fourier frequency and on the energy bands considered (Miyamoto et al. 1988; Vaughan & Nowak 1997; Nowak et al. 1999; Poutanen 2001; Pottschmidt et al. 2003).

The hard and hard-intermediate states are prominent because it is in these states that a compact, optically thick, mildly relativistic jet is detected in the radio band (Fender et al. 2009), hence the relation between accretion and outflow in accreting black holes can be best studied. For the formation and destruction of jets in black-hole and neutron star binaries, the reader is referred to

Kylafis et al. (2012). For an interpretation of the observed phenomenology of black-hole X-ray transients the reader is referred to Kylafis & Belloni (2015).

In a series of papers, we have developed a model for the hard state of BHB. We have shown that Compton upscattering in the jet of soft photons from the accretion disk can explain a number of observational relations between the spectral and timing parameters. Our results demonstrate that jets play a central role in all the observed phenomena, not only in the radio emission.

In Reig et al. (2003) (hereafter Paper I), we reproduced the X-ray energy spectra and the dependence of time lag on Fourier frequency and investigated how the optical depth and extent of the base of the jet affect the spectral continuum. For simplicity, we assumed that the jet has a constant flow velocity v_{\parallel} and in the rest frame of the flow the electrons are mono-energetic, with a velocity component perpendicular to the magnetic field v_{\perp} . The observed parabolic shape of the jet implies that the density of the electrons in the jet drops inversely proportional to the vertical distance z from the black hole.

Giannios et al. (2004) (hereafter Paper II) showed that both the hardening of the high-frequency power spectra and, equivalently, the narrowing of the auto-correlation function with photon energy observed in Cygnus X-1 can be explained by simply assuming that the electrons close to the core of the jet are more energetic than those at its periphery. Specifically, v_{\perp} was assumed to drop linearly with polar distance from the axis of the jet.

In order to explain the entire spectrum from radio to X-rays, Giannios (2005) (hereafter Paper III) assumed that the electrons have a power-law energy distribution. This assumption helps explain the radio part of the spectrum, but has no effect on the Comptonization. This is because the distribution is steep and Comptonization is practically performed by the electrons with the lowest Lorentz factor γ_{\min} .

In Kylafis et al. (2008) (hereafter Paper IV), the correlation observed in Cyg X-1 between the photon index Γ and the average time lag was explained without any additional modification to the model. Similarly for the correlation between Γ and the characteristic frequencies of the Lorentzian peaks (Pottschmidt et al. 2003).

In this work, we aim at reproducing the correlation between the cutoff energy E_c and the phase lag ϕ_{lag} between hard and soft photons, as measured for the BHB GX 339–4 with no or minimal modifications to our jet model. Motta et al. (2009) studied the evolution of the high-energy cut-off in the X-ray spectrum of GX 339–4 across a hard-to-soft transition and found that the cut-off energy decreased monotonically from 120 to 60 keV during the brightening of the hard state. Altamirano & Méndez (2015) studied the evolution of the phase lag of GX 339–4 as a function of the position of the source in the hardness-intensity diagram (q -diagram) and found that the phase lag increases as the sources moves up in the q -diagram through the hard state. They also showed that E_c and ϕ_{lag} appear to be correlated.

In § 2 we present our model briefly, in § 3 we give the results of our calculations, in § 4 we discuss our results, and in § 5 we draw our conclusions.

2. The model

One of the models that we used in this work (model 1) is a simplified version of that used in Paper III. Since we are not interested in reproducing the radio spectrum of GX 339–4, we have

assumed mono-energetic electrons in the jet with Lorentz factor equal to the smallest in the distribution, namely

$$\gamma_{\min} = \frac{1}{\sqrt{1 - (v_{\parallel}^2 + v_{\perp}^2)/c^2}}, \quad (1)$$

where $v_{\parallel} = v_0 = \text{constant}$ is the flow velocity of the jet and v_{\perp} is the smallest perpendicular velocity of the electrons in the rest frame of the flow. As such, our model is identical to that used in Paper IV.

Simplicity is a preferred quality in models, but there are limits. In our model 1 above, we have assumed that the flow velocity in the jet is $v_0 = \text{constant}$ throughout the jet, or equivalently that the acceleration region of the jet is infinitesimal. This is an unphysical description of the base of the jet. For this reason, we have considered a second model (model 2), where the flow velocity in the jet is given by

$$v_{\parallel}(z) = \begin{cases} (z/z_1)^p v_0 & \text{if } 0 < z \leq z_1 \\ v_0 & \text{if } z > z_1, \end{cases} \quad (2)$$

where z_1 and p are parameters. In other words, the jet has an acceleration region of thickness z_1 beyond which the flow has constant velocity v_0 , equal to that of model 1.

For a parabolic jet, i.e. one whose radius at height z is $R(z) = R_0(z/z_0)^{1/2}$, the electron density in model 1 is inversely proportional to z , namely $n_e(z) = n_0(z_0/z)$ (see Paper IV), while in model 2 it is obtained from the continuity equation.

The fixed parameters of our models and their reference values are: the radius $R_0 = 100r_g$ of the base of the jet, where $r_g = GM/c^2$ is the gravitational radius of the black hole, the distance $z_0 = 5r_g$ of the bottom of the jet from the black hole, the height $H = 10^5 r_g$ of the jet, the velocity $v_0 = 0.8c$ of the jet, the thickness $z_1 = 50r_g$ of the acceleration zone, the exponent $p = 0$ (model 1) or $p = 1/2$ (models 2), and the temperature $T_{bb} = 0.2$ keV of the soft-photon input.

The parameters of our models that we have varied are: either the Thomson optical depth along the axis of the jet $1 \leq \tau_{\parallel} \leq 10$ or the minimum Lorentz factor $2 \leq \gamma_{\min} \leq 2.4$ or both with a linear relation between the two. Since v_0 is a constant in our models, the variation of γ_{\min} comes from the variation of $0.35c \leq v_{\perp} \leq 0.42c$.

As the source moves from the hard state to the hard-intermediate one, the jet weakens (Homan & Belloni 2005) and eventually disappears at the jet line. We interpret this weakening of the jet as a decrease of the parameter τ_{\parallel} . At the same time, the luminosity increases, cooling of the jet is enhanced and we interpret this as a decrease of the parameter γ_{\min} . Therefore τ_{\parallel} and γ_{\min} decrease with time during the initial rise of the outburst.

Since the jet is mildly relativistic, the results also depend on the angle θ of observation with respect to the jet axis. As in Papers II–IV, we will focus in an intermediate range of observing angles $0.2 < \cos \theta < 0.6$. Practically, for the Monte Carlo simulation this means that we count only photons that leave the jet in this range of angles.

3. Results

The output of our Monte Carlo code consists of energy spectra and light curves. In this work, the light curves were obtained for the energy bands 2 – 5.7 keV and 5.7 – 15 keV to match those of Altamirano & Méndez (2015) for the BHB GX 339–4.

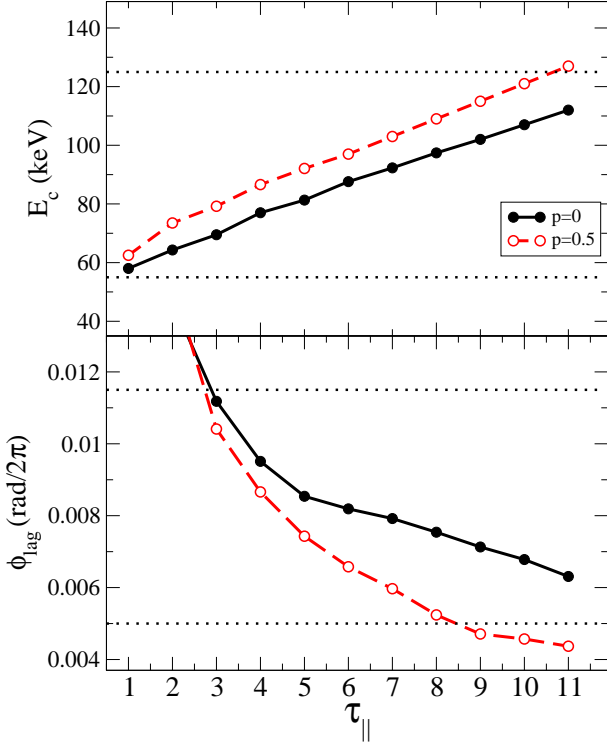


Fig. 1. Cutoff energy and phase lag as functions of τ_{\parallel} when no acceleration zone (filled circles) and when an acceleration zone is included (empty circles). Each point represents a calculation with the same $\gamma_{\min} = 2.28$ ($v_{\perp} = 0.41$) and different τ_{\parallel} . The horizontal dotted lines bracket the ranges of observed values as in Motta et al. (2009) for E_c and Altamirano & Méndez (2015) for ϕ_{lag} .

The output energy spectrum has been fitted by a power-law with an exponential cutoff, to extract the photon index Γ and the cutoff energy E_c . Fourier analysis has been applied to the light curves to obtain the phase lag of the hard X-rays with respect to the soft ones as a function of Fourier frequency. The final phase lag considered, ϕ_{lag} , is the average over the frequency range 0.01 – 5 Hz.

Despite the fact that, in reality, the parameters γ_{\min} and τ_{\parallel} decrease simultaneously, for clarity of presentation, we will first vary τ_{\parallel} , then γ_{\min} , and at the end both. The result that we wish to reproduce in this work is the *decrease* of the cut off energy and the *increase* of the phase lag of GX 339–4 as the X-ray intensity increases and the source traverses the hard state. As explained above, we expect τ_{\parallel} and γ_{\min} to decrease with time. However, for plotting purposes, we left these two parameters, the independent variables of the plots, to increase toward the right in the X-axis, as is normal practice. For this reason E_c *increases* and ϕ_{lag} *decreases* with τ_{\parallel} and γ_{\min} .

3.1. Variation of τ_{\parallel}

In Fig. 1, we show the variations of E_c and ϕ_{lag} as functions of the Thomson optical depth τ_{\parallel} . The solid line represents the case where no acceleration zone is considered (model 1, $p = 0$), while the dashed one represents the case when an acceleration zone is taken into account (model 2, $p = 0.5$). The Lorentz factor of the electrons is fixed at $\gamma_{\min} = 2.24$ ($v_{\parallel} = 0.8c$, $v_{\perp} = 0.395c$) and the rest of the parameters at their reference values. In both panels, the horizontal dotted lines bracket the

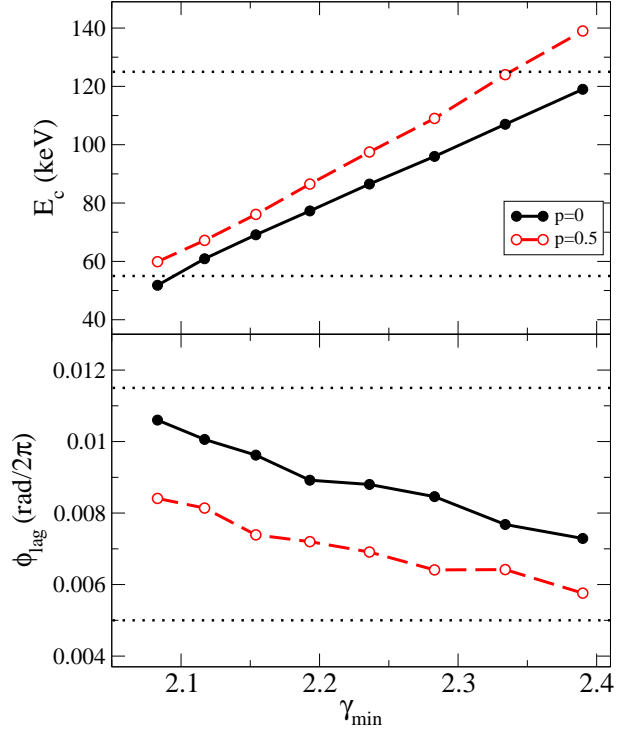


Fig. 2. Cutoff energy and phase lag as functions of γ_{\min} when no acceleration zone (filled circles) and when an acceleration zone is included (empty circles). Each point represents a calculation with the same $\tau_{\parallel} = 5$ and different γ_{\min} (v_{\perp}). The horizontal dotted lines bracket the ranges of observed values as in Motta et al. (2009) for E_c and Altamirano & Méndez (2015) for ϕ_{lag} .

observed values of E_c and ϕ_{lag} , as determined by Motta et al. (2009) and Altamirano & Méndez (2015).

It is important to stress that the variation of E_c and ϕ_{lag} has the correct trend for both model 1 and model 2. On the other hand, variation of only τ_{\parallel} is not enough to reproduce simultaneously the observed ranges of variation of E_c and ϕ_{lag} for the same range of variation of τ_{\parallel} .

Whereas E_c nicely covers the whole range of observed variation when the optical depth τ_{\parallel} decreases from 9 to 1, the phase lag ϕ_{lag} is outside the range of the observations at low optical depths, and lies short at high optical depth. The introduction of an acceleration zone (model 2, $p = 0.5$) makes the ϕ_{lag} trend somewhat steeper, but again the two parameters do not cover the observed ranges of allowed values for the same range of optical depth. Similar curves result for values of p different from 0.5, as long as $p \lesssim 1$.

As it was shown in Papers I–IV, keeping the rest of the parameters to their reference values and decreasing the density n_0 (or equivalently the Thomson optical depth along the axis of the jet τ_{\parallel} , see eq. (2) in Paper IV), makes the emergent spectra softer. A decrease in the optical depth τ_{\parallel} also causes a decrease in the cutoff energy E_c , due to the reduced number of scatterings. The effect on the time lag or the phase lag is, however, less obvious. At large optical depth, the soft input photons penetrate the base of the jet, on average, a skin optical depth of unity. There, they are scattered, but due to the large density, the mean free path is small and the photons sample a small region at the base of the jet before they escape. As the optical depth (or equivalently the density) decreases, the mean free path increases and at small optical depths the photons sample the entire volume of the jet. Thus, the time lag or the phase lag increases.

In the top panel of Fig. 1, one sees that for model 2 ($p = 0.5$) E_c is consistently larger than the corresponding value for model 1 ($p = 0$). This is due to the fact that the mean number of scatterings of the photons in model 2 is larger than that in model 1, which in turn is due to the higher density of the electrons at the base of the jet in model 2 than in model 1.

3.2. Variation of γ_{\min}

In Fig. 2 we show the variation of E_c and ϕ_{lag} as functions of the Lorentz factor γ_{\min} . The optical depth is fixed to $\tau_{\parallel} = 5$ and the rest of the parameters to their reference values. Again, the trend followed by the computed quantities matches that of the observations.

It is natural to expect that E_c would decrease as the energy of the electrons decreases. The increase of ϕ_{lag} as γ_{\min} decreases requires an explanation.

At large γ_{\min} , i.e. large v_{\perp} , there is a tendency for the photons after scattering to have directions with polar angle θ closer to 90 degrees than to zero degrees. Thus, the random walk of the photons occurs close to the base of the jet, and the time lag or phase lag is relatively small, because the size of the jet is small there. As γ_{\min} decreases, i.e. v_{\perp} decreases, the photons after scattering have the tendency to have directions closer to $\theta = 0$ than to $\theta = 90$ degrees. Thus, the input photons are pushed in the flow direction and are forced to sample the entire volume of the jet, which results in relatively larger time lag or phase lag.

As in Fig. 1, only E_c covers the entire range of observed values (indicated by the horizontal dotted lines). The phase lag lies short in one or both of the extremes. The introduction of an acceleration zone (model 2, $p = 0.5$) changes the amplitude of the lags substantially. This is because in the acceleration zone $v_{\parallel} < v_0$ and scattering in directions with θ closer to 90 degrees is enhanced. Thus, the phase lag becomes smaller than in the case of no acceleration zone.

3.3. Variation of τ_{\parallel} and γ_{\min}

Since, in reality, both τ_{\parallel} and γ_{\min} decrease simultaneously as the source moves in the hard state, we varied them both in the simplest way possible, one proportional to the other. In Fig. 3, we show E_c and ϕ_{lag} as functions of τ_{\parallel} . In this Figure, γ_{\min} is linked to τ_{\parallel} by $\gamma_{\min} = 2.023 - 0.019 \tau_{\parallel}$.

With two parameters, τ_{\parallel} and γ_{\min} , working in the same direction, it is not surprising that we have now been able to demonstrate that for $3 \leq \tau_{\parallel} \leq 10$, both computed quantities with model 2, cover simultaneously the entire observed ranges (see the vertical dot-dashed lines in Fig. 3).

To better illustrate the good agreement between the observations and our model, we have plotted the phase lag as a function of the cutoff energy in Fig. 4. The data points come from the works of Motta et al. (2009) and Altamirano & Méndez (2015). The solid and dashed lines corresponds to the models shown in Fig. 3.

4. Summary and conclusion

Observations from space-based X-ray telescopes over the last decades have provided a wealth of data which have led to a revolution in our understanding of black-hole binaries. Numerous studies of these observations have allowed the characterisation of their spectral and temporal properties and the definition of source states. Correlations between the spectral and tim-

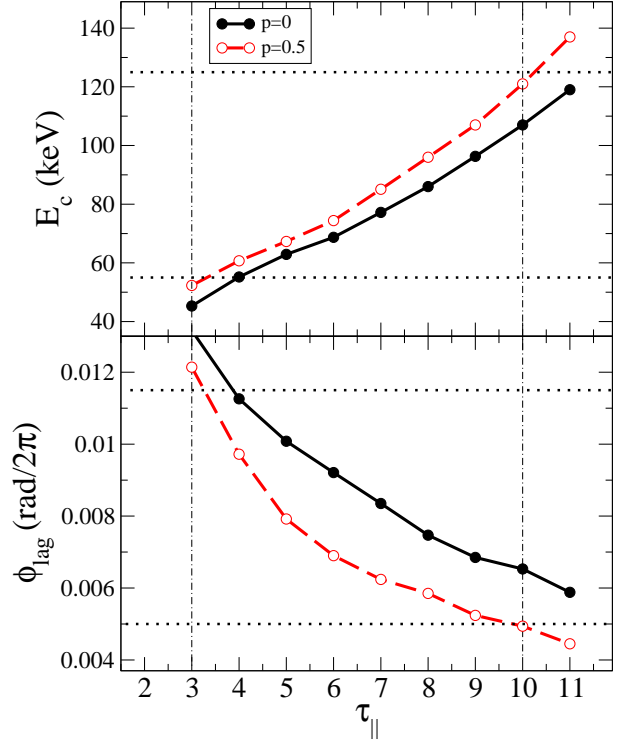


Fig. 3. Cutoff energy and phase lag as a function of τ_{\parallel} when no acceleration zone (filled symbols) and when an acceleration zone is included (open symbols). Each point represents a calculation with different τ_{\parallel} and γ_{\min} . The horizontal dotted lines bracket the ranges of observed values as in Motta et al. (2009) for E_c and Altamirano & Méndez (2015) for ϕ_{lag} . The vertical dot-dashed lines show the range in τ_{\parallel} (hence in γ_{\min} also, see text) where the two quantities cover *simultaneously* the entire observed ranges.

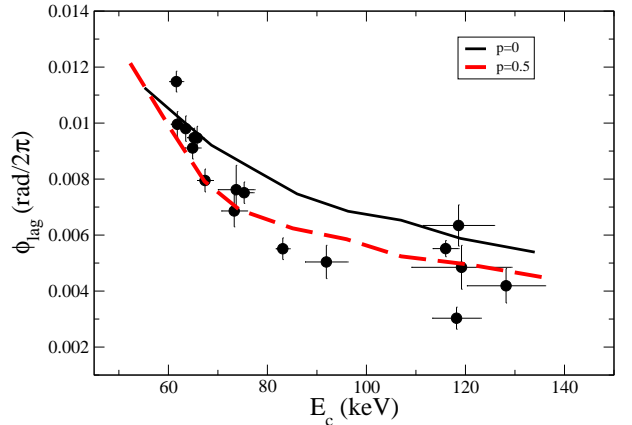


Fig. 4. Phase lags as a function of cutoff energy. Circles represent data from the observations. The cutoff energy and phase lag values were taken from Motta et al. (2009) and Altamirano & Méndez (2015), respectively. Solid and dashed lines correspond to the models shown in Fig. 3.

ing parameters impose tight observational constraints that any model that seeks to explain the observations must address. Our jet model has so far been able to quantitatively explain a number of results regarding the hard state of black-hole binaries (Papers I–IV): *i*) the emergent spectrum from radio to hard X-rays, *ii*) the time(phase)-lags as a function of Fourier frequency, *iii*) the flattening of the power spectra at high frequencies with increasing photon energy and the narrowing of the autocorrelation function,

iv) the correlation observed in Cyg X-1 between the photon index and the average time lag.

The works of Motta et al. (2009) and Altamirano & Méndez (2015) provide one more stringent constraint: the cutoff energy of the power law and the phase lag of hard photons with respect to soft ones vary in unison as the black-hole binary GX 339–4 evolves through the hard state and moves up in the q -diagram (see Fig. 1 in Altamirano & Méndez 2015). In this work, we show that we can reproduce this correlation with a minor modification of our model, namely the introduction of an acceleration zone.

The correlation between the cutoff energy and the phase lag suggests that the most likely origin of the lag is the same region as where the hard X-rays are formed (Altamirano & Méndez 2015). Because the spectrum of the radiation at the energies where the cutoff is measured (tens of keV) cannot be formed in the accretion disk, the $E_c - \phi_{\text{lag}}$ correlation strongly suggests that the lags are due to Comptonization. In our model, Comptonization takes place in the jet. Hence we conclude that the phase lag must originate in the jet. Another result that supports the association between lag and jet stems from the fact that, at least for Cyg X–1, the lag drops as the source moves into the soft-intermediate state (see Fig. 6 in Altamirano & Méndez 2015), that is when the radio emission quenches.

Acknowledgements. We thank the anonymous referee for useful comments and especially for the suggestion of Fig. 4. We acknowledge useful discussions with Dimitrios Gannios. This research has been supported in part by the "RoboPol" project, which is implemented under the "ARISTEIA" Action of the "OPERATIONAL PROGRAM EDUCATION AND LIFELONG LEARNING" and is co-funded by the European Social Fund (ESF) and National Resources.

References

- Altamirano, D. & Méndez, M. 2015, *MNRAS*, 449, 4027
 Band, D. L. & Grindlay, J. E. 1986, *ApJ*, 311, 595
 Belloni, T. M. 2010, in *Lecture Notes in Physics*, Berlin Springer Verlag, Vol. 794, Lecture Notes in Physics, Berlin Springer Verlag, ed. T. Belloni, 53
 Belloni, T. M. & Stella, L. 2014, *Space Sci. Rev.*, 183, 43
 Castro, M., D'Amico, F., Braga, J., et al. 2014, *A&A*, 569, A82
 Dexter, J. & Quataert, E. 2012, *MNRAS*, 426, L71
 Done, C., Gierliński, M., & Kubota, A. 2007, *A&A Rev.*, 15, 1
 Esin, A. A., McClintock, J. E., & Narayan, R. 1997, *ApJ*, 489, 865
 Fabian, A. C., Rees, M. J., Stella, L., & White, N. E. 1989, *MNRAS*, 238, 729
 Fender, R. P., Homan, J., & Belloni, T. M. 2009, *MNRAS*, 396, 1370
 Garain, S. K., Ghosh, H., & Chakrabarti, S. K. 2012, *ApJ*, 758, 114
 Georganopoulos, M., Aharonian, F. A., & Kirk, J. G. 2002, *A&A*, 388, L25
 Ghosh, H., Garain, S. K., Giri, K., & Chakrabarti, S. K. 2011, *MNRAS*, 416, 959
 Giannios, D. 2005, *A&A*, 437, 1007, "Paper III"
 Giannios, D., Kylafis, N. D., & Psaltis, D. 2004, *A&A*, 425, 163, "Paper II"
 Homan, J. & Belloni, T. 2005, *Ap&SS*, 300, 107
 Hua, X.-M. & Titarchuk, L. 1995, *ApJ*, 449, 188
 Kylafis, N. D. & Belloni, T. M. 2015, *A&A*, 574, A133
 Kylafis, N. D., Contopoulos, I., Kazanas, D., & Christodoulou, D. M. 2012, *A&A*, 538, A5
 Kylafis, N. D., Papadakis, I. E., Reig, P., Giannios, D., & Pooley, G. G. 2008, *A&A*, 489, 481, "Paper IV"
 McClintock, J. E. & Remillard, R. A. 2006, *Black hole binaries*, ed. W. H. G. Lewin & M. van der Klis, 157–213
 Merloni, A., Fabian, A. C., & Ross, R. R. 2000, *MNRAS*, 313, 193
 Mitsuda, K., Inoue, H., Koyama, K., et al. 1984, *PASJ*, 36, 741
 Miyamoto, S., Kitamoto, S., Mitsuda, K., & Dotani, T. 1988, *Nature*, 336, 450
 Motta, S., Belloni, T., & Homan, J. 2009, *MNRAS*, 400, 1603
 Narayan, R. & Yi, I. 1994, *ApJ*, 428, L13
 Nowak, M. A., Vaughan, B. A., Wilms, J., Dove, J. B., & Begelman, M. C. 1999, *ApJ*, 510, 874
 Pottschmidt, K., Wilms, J., Nowak, M. A., et al. 2003, *A&A*, 407, 1039
 Poutanen, J. 2001, *Advances in Space Research*, 28, 267
 Reig, P., Kylafis, N. D., & Giannios, D. 2003, *A&A*, 403, L15, "Paper I"
 Remillard, R. A. & McClintock, J. E. 2006, *ARA&A*, 44, 49
 Shakura, N. I. & Sunyaev, R. A. 1973, *A&A*, 24, 337
 Sunyaev, R. A. & Titarchuk, L. G. 1980, *A&A*, 86, 121
 van der Klis, M. 2006, *Rapid X-ray Variability*, ed. W. H. G. Lewin & M. van der Klis, 39–112
 Vaughan, B. A. & Nowak, M. A. 1997, *ApJ*, 474, L43
 Zdziarski, A. A. 1998, *MNRAS*, 296, L51